# Full paper

**DATASET** · OCTOBER 2015

READS
92

**5 AUTHORS**, INCLUDING:

Partho Sarathi Gooh Pattader
Indian Institute of Technology Guwahati
**18** PUBLICATIONS **186** CITATIONS
SEE PROFILE

Ashutosh Sharma IITK
Indian Institute of Technology Kanpur
**335** PUBLICATIONS **7,410** CITATIONS
SEE PROFILE

Langmuir

Article

pubs.acs.org/Langmuir

# Solvent-Vapor-Assisted Dewetting of Prepatterned Thin Polymer Films: Control of Morphology, Order, and Pattern Miniaturization

Nandini Bhandaru,[†] Partho Sarathi Goohpattader,[‡] Danish Faruqui,[‡] Rabibrata Mukherjee,*[,†,‡] and Ashutosh Sharma*[,‡]

[†]Instability and Soft Patterning Laboratory, Department of Chemical Engineering, Indian Institute of Technology Kharagpur, Pin − 721302, Kharagpur, West Bengal, India

[‡]Department of Chemical Engineering and Nanoscience Center, Indian Institute of Technology Kanpur, 208016, Uttar Pradesh, Kanpur, India

Supporting Information

**ABSTRACT:** Ultrathin (<100 nm) unstable polymer films exposed to a solvent vapor dewet by the growth of surface instability, the wavelength ($\lambda$) of which depends on the film thickness ($h_f$). While the dewetting of a flat polymer thin film results in random structures, we show that the dewetting of a prepatterned film results in myriad ordered mesoscale morphologies under specific conditions. Such a film undergoes rupture over the thinnest parts when the initial local thickness of these zones ($h_{rm}$) is lower than a limiting thickness $h_{lim} \approx 10$ nm. Additionally, the width of the pattern grooves ($l_s$) must be wider than $\lambda_s$ corresponding to a flat film having a thickness of $h_{rm}$ for pattern-directed dewetting to take place over surface-tension-induced flattening. We first present an experimentally obtained morphology phase diagram that captures the conditions where a transition from surface-tension-induced flattening to pattern-directed-rupture takes place. Subsequently, we show the versatility of this technique in achieving a variety of aligned mesopatterns starting from a prepatterned film with simple grating geometry. The morphology of the evolving patterns depends on several parameters such as the initial film thickness ($h_f$), prepattern amplitude ($h_{st}$), duration of solvent vapor exposure (SVE), and wettability of the stamp used for patterning. Periodic rupture of the film at regular intervals imposes directionality on the evolving patterns, resulting in isolated long threads/cylindrical ridges of polymers, which subsequently disintegrate into an aligned array of droplets due to Rayleigh−Plateau instability under specific conditions. Other patterns such as a double periodic array of droplets and an array of holes are also possible to obtain. The evolution can be interrupted at any intermediate stage by terminating the solvent vapor annealing, allowing the creation of pattern morphology on demand. The created patterns are significantly miniaturized in size as compared to features obtained from dewetting a flat film with the same $h_f$.

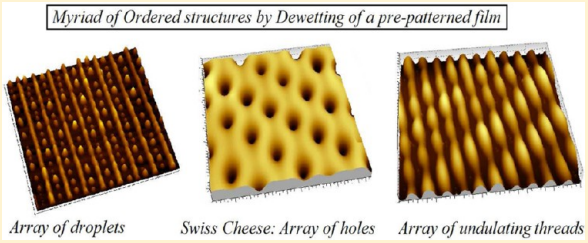


## INTRODUCTION

Ultrathin unstable polymer films rupture spontaneously due to a spinodal instability engendered by the intersurface attractive van der Waals forces.[1−9] Relatively thicker films also often rupture by a heterogeneous mechanism where the surface and the subsurface defects provide the nucleation sites.[3−9] A ruptured film subsequently dewets on a nonwettable substrate by the formation and growth of holes, appearance of rims around them, coalescence of neighboring hole rims, and formation of cellular Voronoi tessellation patterns and their eventual disintegration into isolated, random droplets.[1−9] While the spontaneous disintegration of a film is undesirable from the standpoint of a coating,[10,11] the same phenomenon has the potential to develop into an alternative nonlithographic mesopatterning technique.[12,13] A major advantage of instability-mediated patterning is the ability to tune the morphology, periodicity, and feature size by controlling parameters such as the film thickness ($h_f$) and time and extent of dewetting.[5] However, this approach finds limited application in patterning as the instability-mediated structures are inherently random and therefore has limited utility.[1−9,13] Attempts to overcome this limitation consist of using either a patterned substrate (chemical or topographical) or a confining mold,[14−37] where the imposed lateral confinement leads to ordering of the structures, though the precise alignment mechanism is different in each case. On a chemically patterned substrate, dewetting is engendered by the lateral wettability gradient rather than the nonwettability of the substrate itself; therefore, the film ruptures at the boundaries between the high and low wettability areas. Consequently, the dimensions of the dewetted features as well as the extent of ordering depend on two competing length scales: $\lambda$, the natural instability length scale corresponding to the initial film thickness, and $\lambda_S$, the periodicity of the substrate patterns.[14−18] In contrast, on a topographically patterned substrate, the as-cast film itself has a periodic variation in its local thickness, which is lowest over the substrate protrusions,[19]

**Received:** November 26, 2014
**Revised:** February 15, 2015
**Published:** February 18, 2015





DOI: 10.1021/la5045738
Langmuir 2015, 31, 3203−3214

where the film preferentially ruptures, thereby imposing order on the dewetted patterns.[20−26] However, under strong lateral confinement, aligned droplet formation gets suppressed and the final morphology comprises either undulating threads or large droplets uncorrelated to the substrate features.[26] Ordered instability patterns are also obtained when the film dewets under a patterned mold.[27−36] The experimental configuration in this case is very similar to capillary force lithography (CFL), where pattern replication is achieved by the capillary rise of the polymer meniscus along the contours of the confining stamp and subsequent reorganization under the mold.[37,38] In case the film is not thick enough, there is not adequate polymer for mold filling; consequently, the film undergoes periodic rupture under the stamp, forming aligned threads or ordered droplets.[36]

A closely related and interesting class of problem is the morphological evolution of a patterned thin film when it is subjected to thermal annealing at temperatures above the $T_g$ of the polymer.[39−47] This was first investigated by Buck et al. while exploring the near-surface rheology of polystyrene (PS) films at temperatures slightly below $T_g$. From the rapid decay kinetics of the patterns, they concluded that the local $T_g$ of the film close to the surface is significantly lower than that in the bulk.[39] Jones et al.[40] and Ding et al.[41−43] investigated the influence of polymer viscoelasticity and residual stresses accumulated in a nanoimprinted film by studying the pattern decay of both highly entangled and unentangled polymer thin films using critical dimension small-angle X-ray scattering (CD-SAXS) and specular X-ray reflectivity.[40,41] Cavallini et al. utilized thermal-annealing-induced flattening to obtain an ordered array of nanoscale rings of single molecular magnets on a polymeric surface by controlled demixing.[43] In all of these cases, surface-tension-induced flattening of the film surface (slumping) dominates the initial morphological evolution and the patterned film eventually becomes flat with time. On the basis of the framework of capillary wave theory coupled with linear viscoelastic rheological functions, Rognin et al. presented a model that captures the essential dynamics of slumping.[44] Alvine et al. reported that when a patterned film is annealed at temperatures well above 30−40 K, the $T_g$ of the polymer, for longer durations, the stripes exhibits lateral undulations in addition to pattern-height decay. These undulations grow with time, resulting in the partial coalescence of adjacent stripes.[45] By exposing a nanopatterned film of highly entangled, high-molecular-weight PS to a thermal gradient, Ding et al. identified an influence of elastic recovery in addition to surface tension on the flattening of the film surface in a thin film.[46] They also showed that the zigzag or the out-of-phase undulatory instability in adjacent threads results from an elastic instability and occurs only when the extent of residual stresses is significantly less.[46] On the other hand, in a recent work Bandyopadhyay et al. showed that dewetting is suppressed when the periodicity of the imprinted patterns, $\lambda_P$, is on the order of $\sim{}^1/_{20}$th of the capillary wavelength, as the pattern edges act as truncation points and prevent the propagation of the capillary waves, thereby suppressing film breakup.[47]

In contrast to most of the previously published papers on various aspects of surface-tension-induced flattening,[39−47] we show that a prepatterned film can rupture over the thinnest areas ahead of flattening and produce ordered structures under certain specific conditions. We first identified the necessary conditions that ensure a transition from a flattening-dominated regime to a rupture-dominated regime. We show that for a film to undergo pattern-directed rupture it is necessary that (1) $\lambda_{H\text{-}rm}$ (natural wavelength of instability of a flat film having a thickness $h_{rm}$) be smaller than or of the order of $l_s$ (line width of the grooves) and (2) $h_{rm} \leq h_{lim}$ (critical remnant layer thickness, ∼10 nm). In wider stripes, $l_s \geq \lambda_{H\text{-}rm}$; therefore, the sole condition that determines the evolution is the value of $h_{rm}$; the film flattens out if $h_{rm} > h_{lim}$ and undergoes pattern-directed rupture when $h_{rm} < h_{lim}$. This finding is shown in the form of a morphology phase diagram. Subsequently, we show that by controlling the initial film thickness and the extent of dewetting of a film having grating geometry it becomes possible to create myriad ordered structures by controlling $h_{st}$ (stripe height), the time of dewetting, and the wettability of the stamp used during patterning. The work reported here is significantly distinct from a recent work by Lai and coworkers,[48] where a weak solvent (acetone) is sprinkled onto a patterned polystyrene (PS) film and consequently the morphological evolution is associated with the partial dissolution of the polymer in the solvent, which is largely responsible for the significant spatial variation in morphology observed by the authors.

## MATERIALS AND METHODS

Cleaned 15 mm × 15 mm pieces of a single-side-polished silicon wafer (test grade, Wafer World USA) with a 1.5-nm-thick native oxide layer were used as substrates. For spin coating polystyrene (PS) thin films, 200 μL of a dilute solution of monodisperse PS (MW 280 K, PDI 1.04, Sigma, U.K.) in toluene (HPLC grade, synthesis grade, Merck India) was dispensed on thoroughly cleaned wafer substrates and spun at an RPM of 2500 for 1 min in a spin coater (Apex Instruments, India). The thickness of the films ($h_f$) was controlled by varying the concentration of PS in the dispensed solution and was measured using an imaging ellipsometer (Accuron GmbH, model EP3SW, 532 nm laser source). After coating, the films were air dried for 3 h, followed by annealing in a vacuum oven at 60 °C for 6 h to remove any remnant solvent. Depending on the height of the imprinted stripes ($h_{st}$), $h_f$ was so chosen that $h_{rm}$ after patterning was in the range of 8−10 nm. Control experiments confirmed that patterned films with $h_{rm}$> 12 nm did not rupture and flattened out upon SVE, irrespective of the pattern periodicity ($\lambda_{st}$).

The stamps used for patterning the films had line and groove grating patterns and were fabricated by replica molding Sylgard 184 (a two part cross-linkable siloxane elastomer, Dow Corning, USA) against the polycarbonate part of commercially available optical data discs such as CD ($\lambda_{st}$ = 1.5 μm, $l_s$ = 750 nm) and DVD ($\lambda_{st}$ = 750 nm, $l_s$ = 400 nm) as well as optical gratings ($\lambda_{st}$ = 3.0 μm, $l_s$ = 1.5 μm). Stamps with different $h_{st}$ values were fabricated following a protocol described elsewehere.[49] The different nomenclatures used to identify various dimensions of a prepatterned film are shown in Figure 1.

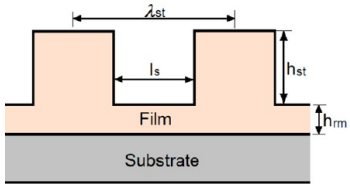


**Figure 1.** Schematic of the prepatterned film with nomenclature.

Cross-linked Sylgard 184 has low surface energy ($\gamma_S$ = 21.7 mJ/m$^2$, measured using a Ramé-Hart model 290 contact angle goniometer) and does not favor the capillary-driven rise of a polymer meniscus during pattern replication. A higher-surface-energy stamp favors capillary-driven flow of the softened polymer layer along the stamp wall. This was achieved by exposing the patterned side of the Sylgard 184 stamps to UV−ozone for 20 min in a UV−ozone chamber (PSD Pro UV−O, Novascan, USA). UV irradiation at 185 nm wavelength produces ozone from the oxygen present in the atmosphere, which


DOI: 10.1021/la5045738
Langmuir 2015, 31, 3203−3214

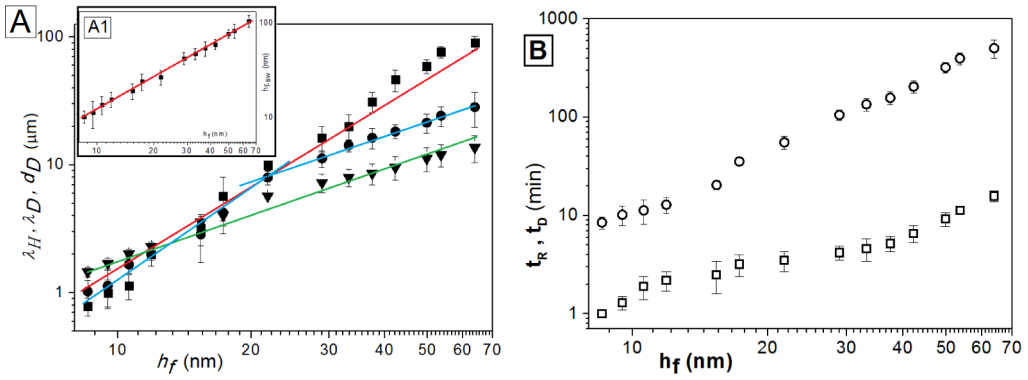


**Figure 2.** (A) Variation of the mean wavelength of holes ($\lambda_H$, ■), the mean wavelength of dewetted droplets ($\lambda_D$, ●), and the mean dewetted droplet diameter ($d_D$, ▼) as a function of film thickness ($h_f$). The lines represent the best-fit data with following functionalities: $\lambda_H \approx h_f^{2.3\pm0.1}$, $\lambda_D \approx h_f^{2.2\pm0.2}$ (for $h_f \leq 21.8$ nm), $\lambda_D \approx h_f^{1.4\pm0.3}$ (for $h_f \geq 21.8$ nm), and $d_D \approx h_f^{1.4\pm0.1}$. Inset A1 shows the swelled film thickness ($h_{f\text{-}sw}$) during SVE as a function of the as-cast film thickness ($h_f$) with a variation of $h_{f\text{-}sw} \approx h_f^{1.1\pm0.1}$. (B) Variation of time of rupture ($t_R$) and time of complete dewetting ($t_D$) of flat films as a function of $h_f$.

subsequently dissociates into atomic oxygen via 254 nm irradiation. The atomic oxygen reacts with the silicone-based Sylgard 184 (cross-linked PDMS) and forms a stiff surface layer of silicon oxide with higher $\gamma_S$ (59.2 mJ/m$^2$).[50]

For prepatterning of the PS films, the Sylgard 184 stamps after UV exposure were brought into conformal contact with the spin-coated PS films. The cross-linked PDMS (polydimethylsiloxane) stamps are compliant in nature, which facilitates conformal contact with the PS films during pattern replication. A gentle compression from the top of the stamp ensured conformal contact between the two. This assembly was then kept in a vacuum oven at 120 °C ($T_g$ of PS 105 °C) for pattern replication to take place, after which the films were cooled to room temperature and the stamps were manually peeled off. The coefficients of thermal expansion of Sylgard, PS, and silicon are significantly different; therefore, high-temperature annealing for pattern replication was avoided. At a lower patterning temperature, the viscosity of the polymer is relatively high; therefore, it takes a longer time for the patterns to replicate. The annealing duration for the films was varied between 3 and 36 h. Depending on the time of pattern replication, partial or complete mold filling was achieved. While a perfect negative replica of the stamp was obtained in the latter case, an intermediate structure comprising a "W" cross section bearing the typical signature of a transient rising meniscus along preferentially wetted confining walls was obtained when the pattern replication time was short.[38] In some cases, a Sylgard stamp without UVO exposure was used for patterning as well. To compensate for the reduced capillary driving force and facilitate pattern transfer, a weight of 100 g evenly distributed over the entire stamp surface was used.

For dewetting, the patterned PS films were exposed to solvent vapor by placing the samples in an airtight chamber presaturated with toluene vapor, which is a good solvent for PS.[52−55] The experimental chamber had a glass cover for viewing and was mounted on the $X$−$Y$−$Z$ stage of an optical microscope (Leica DM 2500) for in situ observations, using white light in reflection mode. After definite durations of exposure, the samples were withdrawn from the chamber and imaged with an AFM (Pico View 5100, Agilent Technologies, USA) in intermittent contact mode with silicon cantilevers (PPP−NCL).

## ■ RESULTS AND DISCUSSIONS

**Morphological Evolution of Flat Films.** To understand the influence of the imprinted patterns on the morphology of the dewetted features as well the kinetics of the dewetting process, we first examine SVE-induced dewetting of flat PS films having a thickness ($h_f$) in the range of 8.3 to 63.9 nm. The dewetting of a polymer film (particularly PS) on a flat substrate has been a subject of extensive study;[2−9] therefore, images of the evolution sequence are not shown. However, we do highlight some of the critical issues which are relevant to the present work. For ultrathin films, usually dewetting is by a spinodal mechanism, whereas slightly thicker films ($h_f \geq 20$ nm) are also influenced by the nucleative mechanisms.[6,8,9] However, in both the cases, the length scale of the instability ($\lambda_H$), which is quantified as the mean separation distance between the holes scales with the film thickness and is shown in Figure 2.[5,6,9] With time more number of holes nucleate, while the existing holes grow in size due to outward retraction of the contact line. Typically, a thick rim surrounds each growing hole, which forms as a consequence of a mismatch between the rates at which polymer is dislodged from the substrate and redistributed to other intact parts of the film.[2−9] Eventually the rims of the adjacent growing holes merge, forming a cellular network of polymer threads. These threads upon prolonged SVE disintegrate into isolated droplets due to a Rayleigh instability.[5,50] It is interesting that the mean separation of the dewetted droplets ($\lambda_D$) is different from $\lambda_H$ as each thread disintegrates into several droplets during Rayleigh instability-mediated disintegration.[5,50] In addition, the retracting rim often exhibits a secondary instability of the contact line, which is particularly prominent in thickener films and results in the detachment of droplets directly from the contact line ahead of the cellular structure formation. Consequently, in all cases $\lambda_D$ is seen to be lower than $\lambda_H$.

The variation of $\lambda_H$, $\lambda_D$, and $d_D$ (the mean droplet diameter) with $h_f$ is shown in Figure 2A, and their functional dependence on $h_f$ is obtained from the best fit to the respective data on a double-logarithmic plot (marked in Figure2A). The scaling relations, which are mentioned in the caption of Figure 2A, match well with previously reported data on SVE[52] as well as thermal dewetting by other groups.[5]

Figure 2A shows a clear transition in the variation of $\lambda_D$ with $h_f$ at around $h_f$ = 22 nm, which we attribute to the absence or appearance of a secondary instability in the rims below and above this particular $h_f$. We argue that slower dynamics in thicker films allows more time for the instability to set along the periphery of the rims and make them undulate. As the drops start to detach from the retracting rim, their number density increases, reducing the rate of increase of $\lambda_D$ with $h_f$. The fingering instability also introduces significant variation of the mean drop size, which is responsible for the larger error bars associated with $d_D$ for greater values of $h_f$. In Figure 2B, we have


DOI: 10.1021/la5045738
Langmuir 2015, 31, 3203−3214

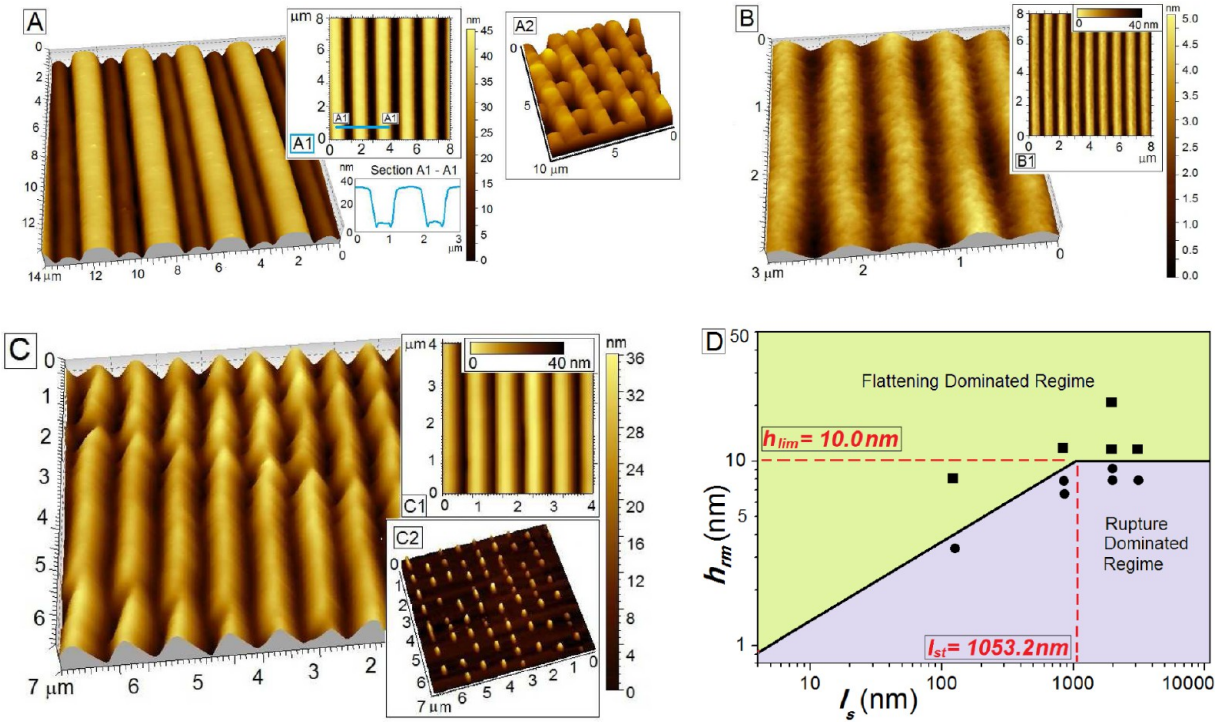


**Figure 3.** (A) Morphology of a ruptured film with $\lambda_{st}$ = 3.0 $\mu$m, $l_s$ = 1.5 $\mu$m, $h_{st}$ = 65 nm, and $h_{rm} \approx$ 8.5 nm after 7 min of SVE. Inset A2 shows the morphology comprising droplets isolated by intact threads after 220 min of SVE. (B) A flattened film after 5 min of SVE. In this case, $\lambda_{st}$ = 750 nm, $l_s$ = 400 nm, $h_{st}$ = 40 nm, and $h_{rm} \approx$ 8.5 nm. (C) Ruptured film with undulating isolated stripes after 4 min of SVE. In this case, $\lambda_{st}$ = 750 nm, $l_s$ = 400 nm, $h_{st}$ = 30 nm, and $h_{rm} \approx$ 4.5 nm. Inset C2 shows the final morphology comprising an aligned array of droplets after 120 min of SVE. (D) Morphology phase diagram identifying the rupture- and flattening-dominated regimes. The experimental data is also shown with squares representing cases where the film flattens out and circles when the film undergoes pattern-directed rupture. Insets A1, B1, and C1 show the initial morphology of the film after patterning.

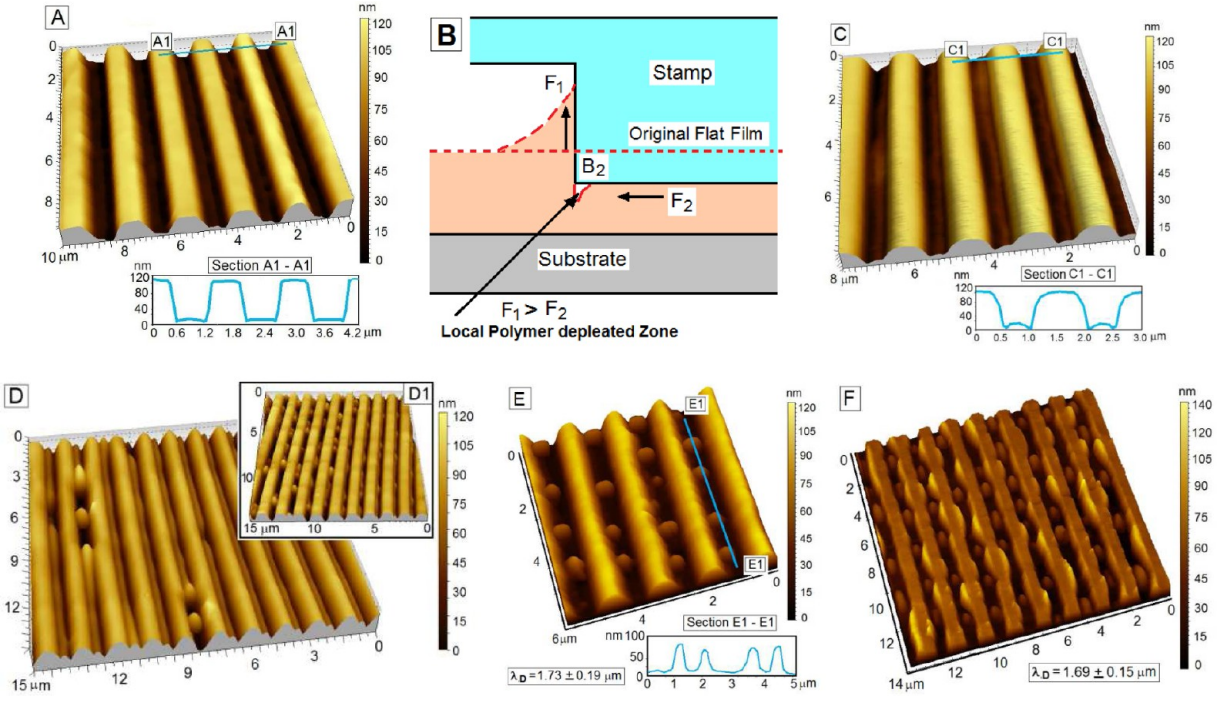


**Figure 4.** (A) Morphology of the patterned film with $\lambda_{st}$ = 1.5 $\mu$m, $l_s$ = 750 nm, $h_{st}$ = 115 nm, and $h_{rm}$ = 8.5 nm. (B) Schematic representing the replication mechanism resulting in a remnant layer with a depleted edge. Morphology of the film (C) after 4 min of SVE, (D) after 21 min of SVE (inset D1 shows morphology comprising more droplets after 30 min of SVE), (E) after 40 min of SVE, and (F) after 200 min of SVE.

plotted the increase in the time of initial rupture ($t_R$) and complete dewetting ($t_D$) with $h_f$. The very long time scales for complete dewetting can be attributed to the high molecular weight of the polymer used in the present study, which makes



DOI: 10.1021/la5045738
*Langmuir* 2015, 31, 3203−3214

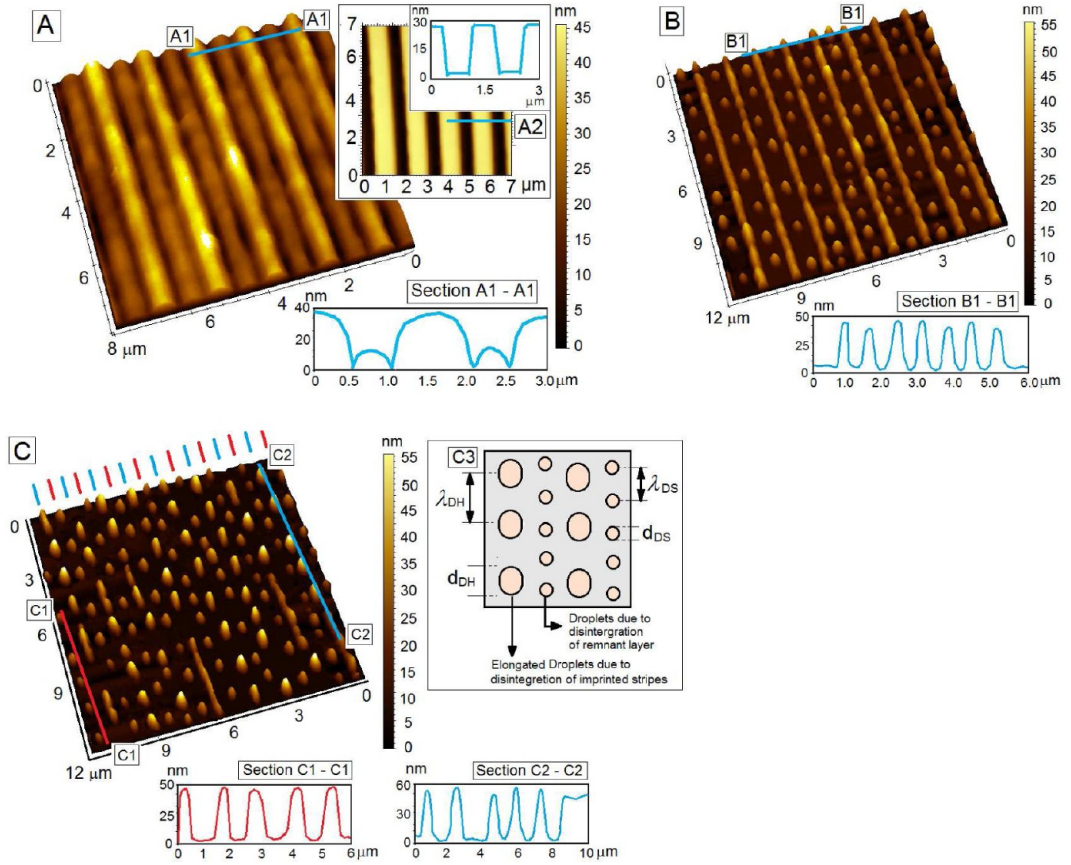


**Figure 5.** Morphological evolution sequence for films with lower $h_{st}$ = 30 nm. (A) After 6 min of SVE, the formation of alternating liquid threads. Inset A1 shows the morphology of the patterned film along with a cross-sectional line scan before solvent vapor exposure. (B) After 32 min of SVE, disintegration into droplets. (C) Final morphology after 400 min of SVE. $\lambda_{st}$, $l_s$, and $h_{rm}$ are the same as in Figure 4. Inset C3 schematically shows the geometry of the final structure to emphasize the genesis of a specific droplet array.

the film kinetically stable for short durations of SVE. However, it must be highlighted that both $t_R$ and $t_D$ are even longer in thermal annealing. For example, we noted $t_D$ = 16 and 56 h for films with $h_f$ = 28.9 and 63.9 nm, respectively, when annealed at 125 °C, in contrast to complete dewetting after 1 h 45 min and 8 h 30 min of SVE, respectively. A faster rate of dewetting in SVE is generally attributed to the rapid penetration of the solvent molecules into the film matrix, which transforms the rheology of the film to a liquidlike (low-viscosity) state with reduced cohesive interaction between adjacent molecules.[52−58] This implies that the actual film thickness during dewetting is greater than $h_f$. Though we have plotted the data in Figure 2A,B as a function of $h_f$ (following the general convention), we did measure the actual swelled film thickness ($h_{f\text{-}sw}$) just ahead of film rupture by performing the SVE on the stage of an ellipsometer, following a protocol described elsewhere.[58]

**Effect of Competing Length Scales on Pattern-Directed Dewetting.** We first investigate the conditions under which the film undergoes pattern-directed dewetting and does not flatten out due to surface tension, which is widely reported.[39−44] Initial pattern-directed rupture over the thinnest zones of the imprinted film is essential to achieving aligned structures, as no ordering is possible when the initial morphological evolution is dominated by flattening. However, once a film has ruptured along the contours of the surface patterns, it cannot flatten out as surface tension can only stabilize an intact film. In fact after rupture, the surface tension aids the retraction of the contact line.[59]

On the basis of several experiments, we found out that morphological evolution on SVE is dominated by pattern-directed rupture when the thickness of the remnant layer ($h_{rm}$) is on the order of 10 nm or lower. We term this $h_{lim} \approx 10$ nm, which is the limiting value of $h_{rm}$. Our experiments showed that films with $\lambda_{st}$ = 1.5 and 3.0 $\mu$m undergo pattern-directed rupture as long as $h_{rm} \leq 10$ nm, irrespective of the $h_{st}$ of the patterns, which can be seen in Figures 3A,C, 4C, 5A, 6B, and 7A. For example, Figure 3A shows that a patterned film with $\lambda_{st}$ = 3.0 $\mu$m ruptures along the striped edges after 7 min of SVE. An identical initial morphology is seen in Figure 4A for a film with $\lambda_{st}$ = 1.5 $\mu$m. In both cases, $h_{rm}$ is ~8.5 ± 0.2 nm and is lower than $h_{lim}$. We observed that films with $h_{rm} \geq 10$ nm flatten out when subjected to SVE, which can be seen in Figure S1 in the Supporting Information. However, even when $h_{rm} <$ 10 nm, a film with $\lambda_{st}$ = 750 nm, $l_s$ = 400 nm, $h_{st}$ = 40 nm, and $h_{rm} \approx 8.5$ nm is seen to flatten out after SVE for 5 min and does not undergo pattern-directed rupture (Figure 3B). Similar flattening is observed in all films with identical $\lambda_{st}$, $l_s$, and $h_{rm}$ and different $h_{st}$ varying between 20 and 100 nm. Further experiments with films having $\lambda_{st}$ = 750 nm and $l_s$ = 400 nm (as before) but with a reduced $h_{rm} \approx 4.5$ nm show pattern-directed rupture in Figure 3C. The isolated threads eventually disintegrate to aligned droplets which are shown in inset C2 of the figure, following a mechanism discussed later in the context of Figure 6B. The above observations make it clear that the condition of $h_{rm} \leq 10$ nm is not adequate to completely



DOI: 10.1021/la5045738
Langmuir 2015, 31, 3203−3214

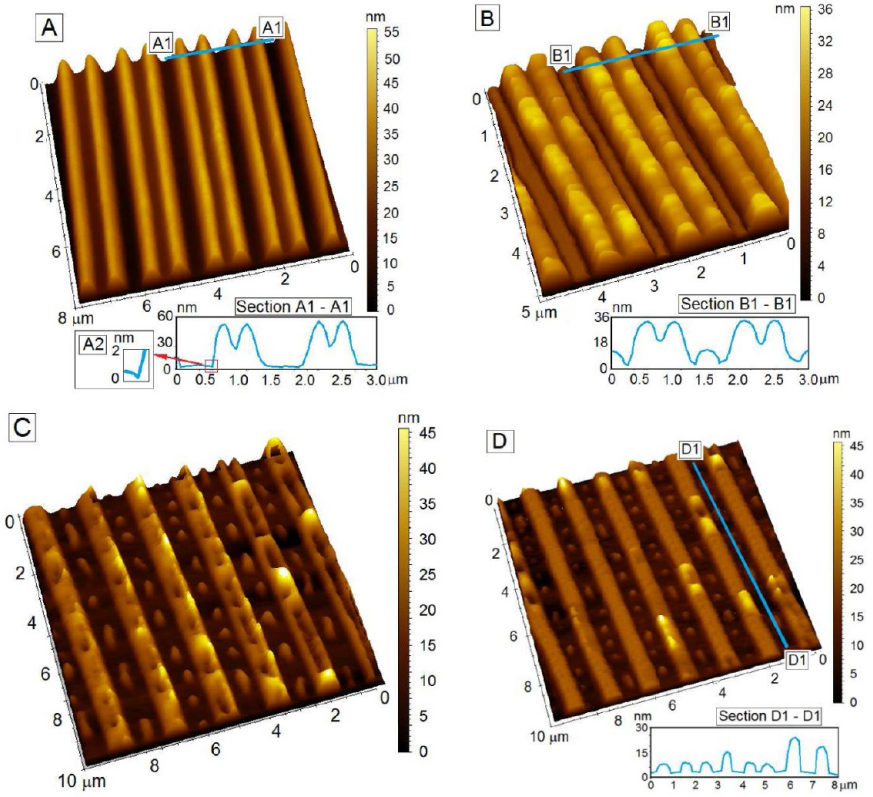


**Figure 6.** (A) Morphology of a patterned film containing W cross-section stripes resulting from incomplete replication during CFL. Inset A2 shows a subtle depression close to the stripe edge. Inset A2 shows the locale-reduced thickness zone along the groove edges. (B) Morphology of the film after 15 min of SVE comprising isolated shallow threads between two adjacent double periodic stripes which have flattened out due to the inward flow of polymer. (C) After 30 min of SVE, the morphology comprises an array of aligned droplets separated by holey threads, due to partial joining of the edges of the sharp W profile double periodic stripes. (D) Final morphology after 190 min of SVE, comprising an array of droplets separated by stable polymer threads. For the film, $\lambda_{st}$ = 1.5 $\mu$m, $l_s$ = 750 nm, $h_{st}$ = 60 nm, and $h_{rm}$ = 8.5 nm.

ensure pattern-directed dewetting over surface-tension-induced flattening, particularly when $l_s$ is progressively reduced.

To gain insight, we focus our attention on natural instability wavelength $\lambda_H$ of a flat film corresponding to the thickness of $h_{rm}$. From Figure 2A, we note that $\lambda_H \approx 730$ nm for a film with $h_f \approx 8.5$ nm. This implies that in prepatterned films having $\lambda_{st}$ = 1.5 $\mu$m (CD stamp) and $\lambda_{st}$ = 3.0 $\mu$m (optical grating stamp), $l_s$ (750 nm and 1.5 $\mu$m, respectively) is wider than $\lambda_{H\text{-}rm}$ (~730 nm). In contrast, the film which is seen to flatten out in Figure 3B has $l_s$ = 400 nm, which means that $\lambda_{H\text{-}rm} > l_s$. In Figure 3C, as $h_{rm}$ is reduced to 4.5 nm, there is an associated lowering of $\lambda_{H\text{-}rm}$ to ~149.3 nm (calculated from the predicted scaling relation of $\lambda_H \approx h_f^{2.3}$ in Figure 2A), which again becomes lower than $l_s$, and the film is seen to undergo pattern-directed dewetting. This observation allows us to emphatically conclude that the necessary condition for a film to undergo pattern-directed rupture is $\lambda_{H\text{-}rm} < l_s$, as long as $h_{rm} < h_{lim}$ (~10 nm). For $h_{rm} > h_{lim}$, a film undergoes flattening irrespective of the relative magnitude of $\lambda_{H\text{-}rm}$ and $l_s$, as higher $h_{rm}$ significantly increases the time of rupture (Figure 2B) and thus offers adequate time for surface tension to flatten the intact film.

On the basis of this understanding, we have constructed a morphology phase diagram in Figure 3D that helps in identifying initial conditions that lead to pattern-directed rupture or flattening as a function of $l_s$ and $h_{rm}$. For $l_s \leq l_{st}$, the boundary between the two regimes is obtained by plotting and joining the points from scaling relation $\lambda_H \approx h_f^{2.3}$ by setting $\lambda_H = l_s$ and $h_f = h_{lim}$. The experimental points are also marked on the plot. We argue that for $h_{rm} \geq h_{lim}$, the subcapillary wavelength patterns on the film surface interrupt the propagation of the capillary waves that have a wavelength corresponding to the thickness of the remnant layer ($\lambda_{H\text{-}rm}$), which are essential for the rupture of the film along the substrate grooves. As a consequence, the film undergoes lateral-confinement-induced stabilization and eventually flattens out. This observation is commensurate with that observed by Karim et al., who reported that a nanoimprinted PS film confined under a cross-linked PDMS stamp becomes stable during thermal annealing when $\lambda_{st} \leq (^1/_{10})\lambda_H$, as the pattern edges truncate the capillary waves and prevent their growth in the presence of the high elastic-energy penalty associated with the deformation of the confining stamp.[47] Our experiments further reveal that $h_{st}$ has no influence on the stability and the initial morphological evolution of the films and controls only the late-stage morphology in the event the film undergoes pattern-directed rupture. The phase diagram in Figure 3D is also independent of the wettability of the stamp used for patterning, which also influences the morphology of the dewetted patterns only and not the regime crossover.

**Morphological Evolution of Films Patterned with Wettable Stamps.** In this section, we investigate how the morphology of the ruptured films evolve as a function of the duration of SVE, $h_{st}$, and the wettability of the stamp used for patterning. Figure 4 shows the morphological evolution sequence of a prepatterned film where $h_{st} \approx 115$ nm and $h_{rm} \approx 8.5$ nm, created by patterning a flat film having $h_f$ = 62.3 ±



DOI: 10.1021/la5045738
Langmuir 2015, 31, 3203−3214

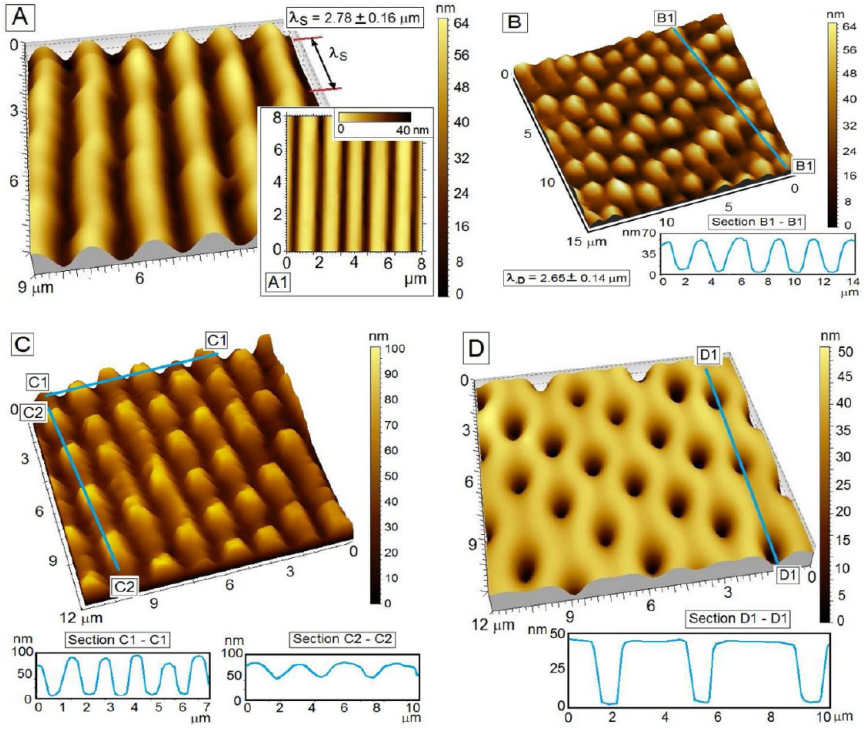


**Figure 7.** Morphological evolution sequence when a nonwettable stamp is used for patterning PS film. Dewetted morphology of a film with (A) $h_{st}$ = 60 nm after 12 min of SVE. Inset A1 shows the initial morphology of the patterned film with a cross section before SVE. (B) $h_{st}$ = 30 nm after 35 min of SVE. (C) $h_{st}$ = 115 nm after 12 min of SVE. (D) $h_{st}$ = 115 nm after 45 min of SVE. For all cases, $\lambda_{st}$ = 1.5 $\mu$m, $l_s$ = 750 nm, and $h_{rm}$ = 8.5 nm. The initial morphology is nearly identical to that shown in inset A1 in all cases, with varying $h_{st}$.

0.7 nm with a wettable stamp. The morphology of the patterned film before SVE is shown in Figure 4A. The cross-sectional profile in the inset of Figure 4A shows a slight depression (reduced local thickness) near the edges of the grooves in the imprinted film. Figure 4C shows the morphology of the film after 4 min of SVE, where the film has started to rupture along each edge of the groove or the remnant layer. The schematic in Figure 4B qualitatively explains the reason for the formation of local low-thickness zones along the groove edges in the patterned film. $F_1$ and $F_2$ are the two major components of flow during pattern replication by CFL that represent the upward capillary-driven rise of the polymer meniscus along the contours of the confining stamp wall and the outward squeezing flow of polymer under each stamp protrusion, respectively. When a stamp with preferential wettability (UVO-exposed) is used, $F_1$ is relatively higher in comparison to $F_2$, which assumes a lower value as the horizontal squeezing flow is subjected to strong no slip at both the polymer−substrate and polymer−stamp interfaces. A short scaling analysis (presented in the Supporting Information) further quantifies that $F_1 \gg F_2$. As a consequence of this mismatch, there is a net depletion of polymer concentration along the groove edges during pattern replication, resulting in a lower local thickness zone. Control experiments reveal that this reduced thickness zone at the edges does not disappear even after keeping the film under the stamp for a very long duration for pattern replication (we continued for 14 days). This implies that there is almost a jamming of the outward squeezing flow of polymer under the stamp protrusions ($F_2 \rightarrow 0$) as the thickness of the remnant layer becomes very low, probably due to very high shear stress at both film−substrate and film−stamp interfaces due to the high viscosity of the polymer melt. It is also worth highlighting that such reduced thickness zones do not appear if a nonwettable (non-UVO-exposed) stamp is used for patterning, arguably as $F_1$ is not favored due to capillarity in this case. This has a pronounced effect on the morphology of the dewetted film, which is shown later in Figure 7. After 12 min of SVE, the film is seen to rupture along each stripe edge, causing the remnant layer sandwiched between two adjacent imprinted stripes to form isolated shallow threads between them (Figure 4C). The morphology of the film at this stage comprises a parallel array of long polymer threads having alternately low (∼18 nm) and high (∼115 nm) thread heights which correspond to the thin remnant layer and the imprinted ridges, respectively. With further SVE, the shallower threads start to undulate due to the onset of the well-known Rayleigh−Plateau instability engendered by the cross-sectional curvature of the long liquid threads.[50] The width of the shallow threads at the time when undulation sets in is ∼643 ± 5 nm. The amplitude of these undulations grows with time, and the first droplets appear due to the disintegration of the thinner threads after about 21 min of SVE (Figure 4D). As shown in inset D1 of the same figure after 30 min of SVE, the number density of the droplets increases with time. The undulating thinner threads disintegrate completely into reasonably well ordered lines of droplets located between the intact thicker stripes after 40 min of SVE, as seen in Figure 4E. The droplets are nearly spherical ($d_{DS} \approx 711.3 \pm 12.6$ nm) and have a characteristic wavelength or correlation length of $\lambda_{DS} = 1.73 \pm 0.19$ $\mu$m along the direction of the stripes (lateral direction). The disintegration of the threads is associated with the minimization of the total free energy of the threads from $2.80 \times 10^{-14}$ to $9.22 \times 10^{-15}$ J/$\mu$m (detailed calculation in the Supporting Information). According to the linear stability analysis (LSA) of



DOI: 10.1021/la5045738
Langmuir 2015, 31, 3203−3214

infinitely long liquid threads, the characteristic wavelength ($\lambda_T$) of capillary instability is directly proportion to the width of the thread ($l_s$) and is governed by the relation $\lambda_T = 4l_s$, which is valid for both viscous and inviscid liquids.[50] A value of $\lambda_{DS}$ = 1.73 $\mu$m indicates that the shallow threads break down when their width is approximately 450 nm, which is significantly narrower than the original groove width, $l_s$ = 750 nm. This implies that after detachment from the adjacent stripes the remnant layer first dewets inward and then undergoes Rayleigh instability-mediated disintegration. Comparing $\lambda_{DS}$ (1.73 $\mu$m) and $d_{DS}$ (711 nm) with the values of $\lambda_D$ (28.37 $\mu$m) and $d_D$ (13.69 $\mu$m) for a film of the same initial thickness (62.3 nm) in Figure 2A, one can clearly see that more than 1 order of miniaturization in the dewetted feature size has been achieved by prepatterning, in addition to ordering of the structures.

Up to this point, the imprinted strips (taller threads) remain relatively stable without exhibiting any undulation. Beyond this stage, the evolution dynamics becomes very sluggish. While the droplets do not undergo any further shape change, the taller threads slowly start to show undulations along their length due to the Rayleigh instability, which can be seen in Figure 4F after 200 min of SVE. Notably, the undulation in the taller threads is haphazard and is seen to grow only in the areas where the droplets formed due to the disintegration of the shallow threads are absent. This implies that the pre-existing droplets act as a confinement and prevent the growth of the undulations of the adjacent threads. However, what precise mechanism triggers the growth of the undulations in the taller threads only at locations where pre-existing droplets are not present is not exactly clear. Very long SVE ($t_{SV}$ = 500 min) results in coalescence of the undulating threads and the droplets, which eventually reduces the total surface area and results in the formation of random holes that never fully disappear even after 1000 min of SVE. The evolution sequence remains nearly identical in patterned films with $h_{st} \geq 40$ nm.

The evolution sequence becomes more complex when $h_{st} \leq$ 30 nm, as the taller threads also disintegrate into droplets due to the Rayleigh−Plateau instability, resulting in a more complex morphology. The initial evolution sequence is similar to that observed in Figure 4, though the time requirement changes. In the case of a film with $h_{st}$ = 30 nm, the stages with alternating shallow and tall liquid threads (Figure 5A) and aligned droplets isolated by threads (Figure 5B) are reached after 6 and 32 min of SVE, respectively. The droplets in Figure 5B are nearly spherical ($d_{DS} \approx 703.3 \pm 19.4$ nm) and have a correlation length of $\lambda_{DS} = 1.6 \pm 0.1$ $\mu$m. Importantly, in contrast to Figure 4E, where is $l_{st} \approx 750$ nm (identical to $l_s$), in Figure 5B we observe that $l_{st} \approx 507.6 \pm 10.9$ nm ($<l_s$), which indicates that the thicker threads have also retracted inward during SVE while the shallower threads disintegrated completely into droplets. The signature of periodic undulations in the intact threads is also visible in Figure 5B. These undulating threads eventually disintegrate into droplets after approximately 55 min of SVE, forming an additional array of dewetted droplets between two pre-existing droplet arrays. For ease of understanding, the arrangement of the droplets in the final stage is schematically shown in inset C3 of Figure 5C. The morphology comprises an alternating array of larger and smaller droplets, arranged along parallel lines, positioned at the erstwhile locations of the remnant layer and imprinted threads on the patterned film. It is clear that the evolution sequence involves the Rayleigh instability-mediated disintegration of the threads twice, at two distinct time intervals of SVE, as the height of the threads resulting from the remnant layer and the imprinted stripes are different. Detailed image analysis reveals that the droplets originating from the disintegration of the imprinted threads (arranged along the blue lines) are larger ($d_{DH} \approx 786.5 \pm 35.6$ nm), mostly nonspherical (oval) with an aspect ratio of $\sim 2.4 \pm 0.2$ and a correlation length of $\lambda_{DH} = 2.13 \pm 0.29$ $\mu$m (calculated neglecting the thread segments which have not disintegrated), in contrast to more spherical droplets ($d_{DS} \approx 716.2 \pm 17.4$ nm, similar to that observed in Figure 5B) aligned along the red lines that have correlation length $\lambda_{DS} = 1.7 \pm 0.2$ $\mu$m. It can further be seen in Figure 5C that some areas of the threads along the blue lines are intact and did not disintegrate into droplets even after very long SVE (~400 min). We attribute this and the nonspherical shape of the larger droplets to rather strong pinning of the threads and the confining influence of the pre-existing droplets. From the standpoint of creating ordered patterns, both of the structures shown in Figure 5B,C are novel and are not readily fabricated by any top-down lithography technique. For one, this would require a mask or stamp with a complex geometry, rather than a simple stripe grating as used here. Second, a photolithography-type technique, unless of a gray-scale variety, cannot produce droplet-like morphology. Furthermore, the morphological evolution can be arrested at any intermediate stage and the patterns can be made permanent by withdrawing the film from the solvent vapor chamber. Both structures allow significant downsizing as compared to features obtained from the dewetting of a flat film of the same $h_f$, in addition to achieving a bimodal size distribution of droplets in Figure 5C.

Figure 6 shows the morphological evolution of films with a "W" cross section, which result from incomplete replication of the stamp pattern on the film surface during CFL. This is achieved by restricting the time for pattern replication to 3 h only, which is inadequate for complete mold filling. The patterned film comprises double periodic stripes with a W cross section that bears a clear signature of the flow profile during replications with a wettable stamp. The preferentially wettable stamp used for patterning the film shown in Figure 6A has a feature height of 60 nm. The patterned film has a maximum height of 52 nm at the edges of each replicated stripe. As shown in Figure 4B, the polymer meniscus first climbs along the two sides of the stamp groove due to capillarity. This is followed by a gradual increase in the level of liquid in the central region of the stamp groove. As the time for pattern replication is short, the central part of the meniscus fails to rise the full height below the stamp groove; consequently, a W-shaped double periodic cross section results. The AFM cross-sectional line scan in Figure 6A reveals that the height of the central portion of the W cross section is 23.2 nm shallower as compared to the height of the stripe edges. The magnitude of $h_{rm}$ was maintained at ~8 nm, which required a careful choice of $h_f$ = 31.2 nm. The imprinted grooves as usual have reduced thickness zones along their border with the W-shaped stripes, which is seen clearly in inset A2 of Figure 6A.

Upon SVE for 15 min, the remnant layer first detaches from the stripe edges and forms shallow threads between the W-shaped stripes (Figure 6B), following a mechanism discussed earlier. Simultaneously, the sharp edges of the W-shaped stripes start to flatten out rapidly with the flow of polymer toward the inner side of the W-shaped grooves. This flow is triggered by an imbalance in the Laplace pressure, and a negative inward radius of curvature of the W-shaped threads engenders the inward flow. Figure 6B also shows some bright spots along the



DOI: 10.1021/la5045738
Langmuir 2015, 31, 3203−3214

flattened thread edges, which indicate localized polymer accumulation due to the onset of the Rayleigh instability along each arm of the W stripes. Interestingly, in this case the Rayleigh instability sets in along the raised side arms of the W-shaped threads ahead of its onset along the shallow threads, which is in clear contrast to our earlier observations in Figures 4D and 5B. This happens as the local width of the threads at the side edges is narrower than that of the shallow threads; therefore, a higher local curvature favors the early onset of the instability along the stripe edges. However, the instability mode fails to cause any major undulation along the double periodic threads as there is simultaneous liquid flow into the inner grooves and associated flattening. Thus, Figure 6B shows a stage when three distinct flow mechanisms are cooperative, which are (1) the detachment of the remnant layer from the stripes and inward retraction of the contact line, (2) Laplace-pressure-driven flattening of the stripe edges (localized slumping), and (3) the Rayleigh−Plateau instability along the sharp stripe edges. However, the influence of the last mode is rather weak. After 30 min of SVE, the shallow threads disintegrate completely into an array of droplets, while the double periodic stripes join up at many places due to the inward flow of polymer, resulting in a complex morphology comprising an array of droplets separated by polymer threads that contain periodic, nearly equally sized holes (Figure 6C). With time, the holes eventually get filled up and the morphology after 190 min of SVE becomes identical to that seen in Figure 5B, comprising an array of droplets separated by threads (Figure 6D). Beyond this stage, the evolution is identical to that seen in an earlier case, and the morphology becomes similar to that shown in Figure 4F after 720 min of SVE (image not shown).

**Morphological Evolution of Films Patterned with Nonwettable Stamps.** Figure 7 shows the evolution sequence when a nonwettable stamp is used to pattern the PS film. In this case, pattern replication is achieved by viscoplastic deformation of the liquefied polymer film under a low externally applied pressure rather than by a spontaneous capillary-driven rise of the polymer meniscus along the stamp walls. The pattern-replication mechanism in this case is identical to nanoimprint lithography (NIL) using a flexible stamp. The flow during pattern replication is significantly dominated by the outward squeezing flow of the polymer meniscus below the stamp protrusions ($F_2$, Figure 4B).

The inward flow components from opposite directions meet below every stamp groove and trigger an upward flow of polymer in the center of each stamp groove, which eventually leads to mold filling and pattern replication. As a consequence, the local low-thickness zones at the edges of the remnant layer do not form. Instead, $h_{rm}$ is minimum at the center of the remnant layer between two adjacent stripes. Consequently, the film is seen to rupture at the central portion of each groove soon after SV annealing and is seen to result in isolated parallel polymer threads after 5 min of SVE. Figure 7A shows that in a film with $h_{st}$ = 60 nm, these isolated threads starts to undulate due to Rayleigh instability after 12 min of SVE. Up to this stage, the evolution dynamics is independent of $h_{st}$. Beyond this stage, evolution sequence is seen to depend strongly on $h_{st}$. Figure 7B shows that in a film with low $h_{st}$ = 30 nm, the undulation amplitude of the threads progressively increase and leads to complete disintegration of the threads into array of isolated droplets after 35 min of SVE. The droplets have a correlation length of $\lambda_{DS}$ = 2.7 ± 0.1 $\mu$m. The disintegration of the threads into droplets gets progressively suppressed with increasing $h_{st}$, as the advancing undulation fronts of the adjacent stripes join up with each other. This is seen in Figure 7C for a film with $h_{st}$ = 115 nm, where the threads become undulating due to the Rayleigh instability but have not disintegrated into droplets after 12 min of SVE. The figure also shows that in many cases the bulges along adjacent stripes coexist side by side; therefore, the instability mode can be considered to be zigzag or out of phase, as termed by Alvine et al.[48] As the amplitude of the undulations grows with progressive SVE, the adjacent bulges join up with each other and the morphology of the film after 45 min of SVE comprises a well-ordered array of equally sized holes resembling Swiss cheese morphology (Figure 7D). The holes, which have an average diameter of $d_H \approx 892 \pm 16.6$ nm, have a correlation length of $\lambda_H$ = 3.1 ± 0.1 $\mu$m. Prolonged SVE of 600 min beyond this stage leads to the eventual filling up of the holes in favor of a flat film. This film is seen to rupture after about 750 min of SVE, with the formation of random holes noncorrelated to the imprinted structures.

Before concluding, we would like to highlight that the results discussed in this article are not limited to PS film exposed to toluene vapor, as we performed several experiments with patterned PMMA films that were exposed to toluene and chloroform vapor. We observed both flattening and pattern-directed dewetting in the PMMA films, following conditions identified in the morphology phase diagram (Figure 3D) developed by us. Figure S4 in the Supporting Information contains images that show the morphology of prepatterned PMMA thin films exposed to chloroform vapor for different durations. These experiments add generality and highlight the material-independent nature of the observations.

## CONCLUSIONS

The work reported in this article can be broadly subdivided into two parts. In the first part, we have experimentally identified the conditions which distinguish a transition between surface-tension-induced flattening (slumping) and pattern-directed rupture, when a prepatterned polymer film is exposed to its own solvent vapor. Our experiments reveal that the patterned films rupture along the contours of the imprinted features when $h_{rm} \leq 10$ nm. Additionally, $l_s$ must be wider than the natural instability wavelength corresponding to the thickness of the remnant layer ($\lambda_{H-rm} \leq l_s$) in confined films (low $\lambda_{st}$ and low $l_s$). Otherwise, the pre-existing pattern on the film surface interrupts the propagation of the capillary waves and suppresses pattern-directed rupture. It is also seen that $h_{st}$ and the wettability of the stamp used for patterning do not affect the regime crossover and influence only the late-stage morphology and extent of ordering of the dewetted features.

In the second part of the article, we show that myriad ordered mesoscale patterns can be obtained by pattern-directed rupture and dewetting of a patterned thin polymer film with a simple line-and-groove grating geometry. Obtaining ordered patterns which are clearly distinct from being a mere negative replica of the stamp is indeed a key strength of the reported work. Additionally, significant downsizing of the feature geometry, as compared to those obtained from dewetting a flat film of same initial thickness, is also seen in the case of a prepatterned film.

A combination of these two favorable factors offers the potential for this method to be developed into a viable "beyond the master" patterning technique, which combines the essential concepts of top-down and bottom-up approaches. We have



DOI: 10.1021/la5045738
Langmuir 2015, 31, 3203−3214

shown that the morphology of the dewetted patterns and the extent of ordering can be tuned by controlling the initial geometry of the imprinted films ($h_{st}$ and $\lambda_{st}$), the wettability of the stamp used for patterning, and the duration of SV annealing. In all of our experiments, the grating patterned films had a duty ratio of 1 (limited by the availability of stamps). We feel that this might be another important parameter that might significantly influence the dewetting morphology.

As already mentioned, dewetting a thin polymer film on a topographically or a chemically patterned substrate has been the preferred techniques for aligning dewetting features. However, it is important to realize that the ordered dewetting features are obtained on a template, not on a homogeneous substrate. This is the key strength of the work reported in this article, and thus we feel that structures arising out of the approach might find application in several areas. We propose that the dewetted structures can be used as a sacrificial mask for the hydrothermal growth of an oxide layer on FTO-coated glass, which is essential to the fabrication of various sensitized solar cells.[60] The presence of the ordered polymer droplets (even PS or PMMA) is likely to screen the growth of the oxide nanowires, thereby increasing the interfacial area of the active layer significantly. The prepatterning of a P3HT/PCBM layer in an organic photovoltaic solar cell has also been proposed to enhance efficiency. Similar work with a functional polymer might provide clues as to how the morphology of the interface gradually evolves with time and is likely to provide additional clues to enhance cell performance.[61]

## ■ ASSOCIATED CONTENT

### Supporting Information

A short scaling analysis to show the relative magnitudes of $F_1$ and $F_2$ during pattern replication, morphology of dewetted PMMA filmsm, and how surface energy decreases due to the disintegration of a thread into an array of droplets. This material is available free of charge via the Internet at http://pubs.acs.org.

## ■ AUTHOR INFORMATION


### Corresponding Authors

*E-mail: rabibrata@che.iitkgp.ernet.in.
*E-mail: ashutos@iitk.ac.in.


### Notes

The authors declare no competing financial interest.

## ■ ACKNOWLEDGMENTS

We acknowledge the support of the Department of Science & Technology (DST), New Delhi, India for funding the research under its Nano Mission program to IIT Kanpur through its Center for Nanosciences and to IIT Kharagpur by a research grant (SR/NM/NS-63/2010).

## ■ NOMENCLATURE

$d_D$ average dewetted droplet diameter on a flat surface, $\mu$m
$d_{DH}$ average diameter of dewetted droplets arising out of the dewetting of imprinted threads (refer to inset C3, Figure 5), nm
$d_{DS}$ mean dewetted droplet diameter along the stripes, nm
$d_H$ average hole diameter (refer to Figure 7D), nm
$F_1$ capillary-driven upward component of flow during pattern replication
$F_2$ outward squeezing component of flow (horizontal) under stamp protrusion
$h_f$ thickness of spin-cast flat film, nm
$h_{f\text{-}sw}$ thickness of swelled film during solvent vapor exposure, nm
$h_{lim}$ critical remnant layer thickness, ~10 nm
$h_{rm}$ initial remnant layer thickness, nm
$h_{st}$ stripe height on imprinted films, nm
$l_s$ line width on imprinted films, nm
$l_{st}$ critical transition line width, nm
$T_g$ glass-transition temperature of polymer, K
$t_R$ time for initial rupture of a film, min
$t_D$ time for complete dewetting of a film, min

### Greek Letters

$\lambda$ natural length scale of instability in dewetting of a thin film on a flat substrate, nm
$\lambda_D$ periodicity of dewetted droplets on a flat substrate, $\mu$m
$\lambda_{DH}$ periodicity of dewetted droplets arising out of the dewetting of imprinted threads (refer to inset C3, Figure 5), nm
$\lambda_{DS}$ droplet periodicity along the stripes, nm
$\lambda_H$ periodicity of dewetted holes, nm
$\lambda_{H\text{-}rm}$ natural length scale of instability on a flat substrate corresponding to $h_{rm}$, nm
$\lambda_P$ periodicity of imprinted patterns, nm
$\lambda_S$ periodicity of undulations along imprinted threads during SVE, nm
$\lambda_{st}$ periodicity of replicated stripes, nm
$\lambda_T$ wavelength of capillary instability, nm
$\gamma_S$ surface energy, mJ/m$^2$

## ■ REFERENCES


(1) Xie, R.; Karim, A.; Douglas, J. F.; Han, C. C.; Weiss, R. A. Spinodal Dewetting of Thin Polymer Films. *Phys. Rev. Lett.* **1998**, *81*, 1251−1254.

(2) Sharma, A.; Khanna, R. Pattern Formation in Unstable Thin Liquid Films. *Phys. Rev. Lett.* **1998**, *81*, 3463−3466.

(3) Seemann, R.; Herminghaus, S.; Jacobs, K. Dewetting patterns and molecular forces: A reconciliation. *Phys. Rev. Lett.* **2001**, *86*, 5534−5537.

(4) Reiter, G. Dewetting of thin polymer films. *Phys. Rev. Lett.* **1992**, *68*, 75−78.

(5) Sharma, A.; Reiter, G. Instability of Thin Polymer Films on Coated Substrates: Rupture Dewetting, and Drop Formation. *J. Colloid Interface Sci.* **1996**, *178*, 383−399.

(6) Sharma, A. Many Paths to Dewetting of Thin Films: Anatomy and Physiology of Surface Instability. *Eur. Phys. J. E* **2003**, *12*, 397−408.

(7) Reiter, G.; Hamieh, M.; Damman, P.; Sclavons, S.; Gabriele, S.; Vilmin, T.; Raphael, E. Residual Stresses in Thin Polymer Films Cause Rupture and Dominate Early Stages of Dewetting. *Nat. Mater.* **2005**, *4*, 754−758.

(8) Becker, J.; Grün, G.; Seemann, R.; Mantz, H.; Jacobs, K.; Mecke, K. R.; Blossey, R. Complex dewetting scenarios captured by thin-film models. *Nat. Mater.* **2003**, *2*, 59−63.

(9) Verma, R.; Sharma, A. Defect Sensitivity in Instability and Dewetting of Thin Liquid Films: Two Regimes of Spinodal Dewetting. *Ind. Eng. Chem. Res.* **2007**, *46*, 3108−3118.

(10) Barnes, K. A.; Karim, A.; Douglas, J. F.; Nakatani, A. I.; Gruell, H.; Amis, E. J. Suppression of Dewetting in Nanoparticle-Filled Polymer Films. *Macromolecules* **2000**, *33*, 4177−4185.

(11) Roy, S.; Bandyopadhyay, D.; Karim, A.; Mukherjee, R. Interplay of Substrate Surface Energy and Nanoparticle Concentration in Suppressing Polymer Thin Film Dewetting. *Macromolecules* **2015**, *48*, 373−382.




DOI: 10.1021/la5045738
*Langmuir* 2015, 31, 3203−3214

(12) Gentili, D.; Foschi, G.; Valle, F.; Cavallini, M.; Biscarini, F. Applications of Dewetting in Micro and Nanotechnology. *Chem. Soc. Rev.* **2012**, *41*, 4430−4443.
(13) Craster, R. V.; Matar, O. K. Dynamics and Stability of Thin Liquid Films. *Rev. Mod. Phys.* **2009**, *81*, 1131−1198.
(14) Kargupta, K.; Sharma, A. Templating of Thin Films Induced by Dewetting on Patterned Surfaces. *Phys. Rev. Lett.* **2001**, *86*, 4536−4539.
(15) Sehgal, A.; Ferreiro, V.; Douglas, J. F.; Amis, E. J.; Karim, A. Pattern-Directed Dewetting of Ultrathin Polymer Films. *Langmuir* **2002**, *18*, 7041−7048.
(16) Zhang, Z.; Wang, Z.; Xing, R.; Han, Y. Patterning Thin Polymer Films by Surface-Directed Dewetting and Pattern Transfer. *Polymer* **2003**, *44*, 3737−3743.
(17) Wang, X.; Tvingstedt, K.; Inganas, O. Single- and Bilayer Submicron Arrays of Fluorescent Polymer on Conducting Polymer Surface with Surface Energy Controlled Dewetting. *Nanotechnology* **2005**, *16*, 437−443.
(18) Julthongpiput, D.; Zhang, W.; Douglas, J. F.; Karim, A.; Fasolka, M. J. Pattern-Directed to Isotropic Dewetting Transition in Polymer Films on Micropatterned Surfaces with Differential Surface Energy Contrast. *Soft Matter* **2007**, *3*, 613−618.
(19) Roy, S.; Ansari, K. J.; Jampa, S. S. K.; Vutukuri, P.; Mukherjee, R. Influence of Substrate Wettability on the Morphology of Thin Polymer Films Spin-Coated on Topographically Patterned Substrates. *ACS Appl. Mater. Interfaces* **2012**, *4*, 1887−1896.
(20) Rehse, N.; Wang, C.; Hund, M.; Geoghegan, M.; Magerle, R.; Krausch, G. Stability of Thin Polymer Films on a Corrugated Substrate. *Eur. Phys. J. E* **2001**, *4*, 69−76.
(21) Luo, C.; Xing, R.; Zhang, Z.; Fu, J.; Han, Y. Ordered Droplet Formation by Thin Polymer Film Dewetting on a Stripe-Patterned Substrate. *J. Colloid Interface Sci.* **2004**, *269*, 158−163.
(22) Xing, R.; Luo, C.; Wang, Z.; Han, Y. Dewetting of Polymethyl Methacrylate on the Patterned Elastomer Substrate by Solvent Vapor Treatment. *Polymer* **2007**, *48*, 3574−3583.
(23) Rath, S.; Heilig, M.; Port, H.; Wrachtrup, J. Periodic Organic Nanodot Patterns for Optical Memory. *Nano Lett.* **2007**, *7*, 3845−3848.
(24) Yoon, B.; Acharya, H.; Lee, G.; Ho-Cheol, K.; Huh, J.; Park, C. Nanopatterning of Thin Polymer Films by Controlled Dewetting on a Topographic Pre-Pattern. *Soft Matter* **2008**, *4*, 1467−1472.
(25) Mukherjee, R.; Bandyopadhyay, D.; Sharma, A. Control of Morphology in Pattern Directed Dewetting of Thin Polymer Films. *Soft Matter* **2008**, *4*, 2086−2097.
(26) Roy, S.; Mukherjee, R. Ordered to Isotropic Morphology Transition in Pattern-Directed Dewetting of Polymer Thin Films on Substrates with Different Feature Heights. *ACS Appl. Mater. Interfaces* **2012**, *4*, 5375−5385.
(27) Suh, K. Y.; Lee, H. H. Anistropic Hole Formation in Thin Polymer Films Confined by Walls. *J. Chem. Phys.* **2001**, *115*, 8204−8208.
(28) Suh, K. Y.; Lee, H. H. Self-Organized Polymeric Microstructures. *Adv. Mater.* **2002**, *14*, 346−351.
(29) Suh, K. Y.; Park, J.; Lee, H. H. Controlled Polymer Dewetting by Physical Confinement. *J. Chem. Phys.* **2002**, *116*, 7714−7718.
(30) Kim, Y.S.; Lee, H.H. Selective Dewetting for General Purpose Patterning. *Adv. Mater.* **2003**, *15*, 332−334.
(31) Suh, K.Y.; Langer, R. Microstructures of Poly(ethylene glycol) by Molding and Dewetting. *Appl. Phys. Lett.* **2003**, *83*, 1668−1670.
(32) Cavallini, M.; Biscarini, F. Nanostructuring Conjugated Materials by Lithographically Controlled Wetting. *Nano Lett.* **2003**, *3*, 1269−1271.
(33) Zhang, H.L.; Bucknall, D.G.; Dupuis, A. Uniform Nanoscopic Polystyrene Patterns Produced from a Microscopic Mold. *Nano Lett.* **2004**, *4*, 1513−1519.
(34) Luo, C.; Xing, R.; Han, Y. Ordered Pattern Formation from Dewetting of Polymer Thin Film with Surface Disturbance by Capillary Force Lithography. *Surf. Sci.* **2004**, *552*, 139−148.
(35) Baralia, G.G.; Filiatre, C.; Nysten, B.; Jonas, A. M. Nanodecoding by Dewetting. *Adv. Mater.* **2007**, *19*, 4453−4459.
(36) Park, H.; Russell, T.P.; Park, S. Spatial Control of Dewetting: Highly Ordered Teflon Nanospheres. *J. Colloid Interface Sci.* **2010**, *348*, 416−423.
(37) Suh, K. Y.; Kim, Y. S.; Lee, H. H. Capillary Force Lithography. *Adv. Mater.* **2001**, *13*, 1386−1389.
(38) Suh, K. Y.; Yoo, p. J.; Lee, H. H. Meniscus Formation and Breakdown of Thin Polymer Films in Microchannels. *Macromolecules* **2002**, *35*, 4414−4418.
(39) Buck, E.; Petersen, K.; Hund, M.; Krausch, G.; Johannsmann, D. Decay Kinetics of Nanoscale Corrugation Gratings on Polymer Surface: Evidence for Polymer Flow below the Glass Temperature. *Macromolecules* **2004**, *37*, 8647−8652.
(40) Jones, R. L.; Hu, T.; Soles, C. L.; Lin, E. K.; Reano, R. M.; Pang, S. W.; Casa, D. M. Real-Time Shape Evolution of Nanoimprinted Polymer Structures during Thermal Annealing. *Nano Lett.* **2006**, *6*, 1723−1728.
(41) Ding, Y.; Ro, H. W.; Germer, T. A.; Douglas, J. F.; Okerberg, B. C.; Karim, A.; Soles, C. L. Relaxation Behavior of Polymer Structures Fabricated by Nanoimprint Lithography. *ACS Nano* **2007**, *1*, 84−92.
(42) Ding, Y.; Ro, H. W.; Douglas, J. F.; Jones, R. L.; Hine, D. R.; Karim, A.; Soles, C. L. Polymer Viscoelasticity and Residual Stress Effects on Nanoimprint Lithography. *Adv. Mater.* **2007**, *19*, 1377−1382.
(43) Cavallini, M.; Gomez-Segura, J.; Albonetti, C.; Ruiz-Molina, D.; Veciana, J.; Biscarini, F. Ordered Patterning of Nanometric Rings of Single Molecule Magnets on Polymers by Lithographic Control of Demixing. *J. Phys. Chem. B* **2006**, *110*, 11607−11610.
(44) Rognin, E.; Landis, S.; Davoust, L. Viscoelastic Leveling of Annealed Thin Polystyrene Films. *Langmuir* **2014**, *30*, 6963−6969.
(45) Alvine, K. J.; Ding, Y. F.; Douglas, J. F.; Ro, H. W.; Okerberg, B. C.; Karim, A.; Soles, C. L. Capillary Instability in Nanoimprinted Polymer Films. *Soft Matter* **2009**, *5*, 2913−2918.
(46) Ding, Y.; Qi, H. J.; Alvine, K. J.; Ro, H. W.; Ahn, D. U.; Lin-Gibson, S.; Douglas, J. F.; Soles, C. L. Stability and Surface Topography Evolution in Nanoimprinted Polymer Patterns under a Thermal Gradient. *Macromolecules* **2010**, *43*, 8191−8201.
(47) Bandyopadhyay, D.; Singh, G.; Becker, M. L.; Karim, A. Capillary Wave Confinement-Induced Stabilization of Polymer Films. *ACS Appl. Mater. Interfaces* **2013**, *5*, 4006−4010.
(48) Lai, K.-L.; Hsiao, S.-F.; Hon, M.-H.; Leu, I.-C. Patterning of Polystyrene Thin Films by Solvent-Assisted Imprint Lithography and Controlled Dewetting. *Microelectron. Eng.* **2012**, *94*, 33−37.
(49) Bhandaru, N.; Roy, S.; Suruchi; Harikrishnan, G.; Mukherjee, R. Lithographic Tuning of Polymeric Thin Film Surfaces by Stress Relaxation. *ACS Macro Lett.* **2013**, *2*, 195−200.
(50) Roy, S.; Bhandaru, N.; Das, R.; Harikrishnan, G.; Mukherjee, R. Thermally Tailored Gradient Topography Surface on Elastomeric Thin Films. *ACS Appl. Mater. Interfaces* **2014**, *6*, 6579−6588.
(51) Rayleigh, L. On the Instability of Jets Proc. *London Math. Soc.* **1878**, *10*, 4−13.
(52) Lee, S. H.; Yoo, P. J.; Kwon, S. J.; Lee, H. H. Solvent-driven Dewetting and Rim Instability. *J. Chem. Phys.* **2004**, *121*, 4346−4351.
(53) Zhang, S.; Shi, T.; You, J.; Li, Y. Solvent annealing induced phase separation and dewetting in PMMA/SAN blend films: composition dependence. *Polym. Chem.* **2013**, *4*, 3943−3948.
(54) You, J.; Zhang, S.; Huang, G.; Shi, T.; Li, Y. Solvent annealing induced phase separation and dewetting in PMMA/SAN blend film: Film thickness and solvent dependence. *J. Chem. Phys.* **2013**, *138*, 244907.
(55) Zhang, S.; Zhu, Y.; Shi, T.; Zhao, H.; You, J.; Li, Y. Selective Solvent Annealing Induced Phase Separation and Dewetting in PMMA/SAN Blend Ultrathin Films. *J. Polym. Sci., Part B: Polym. Phys.* **2014**, *52*, 1243−1251.
(56) Verma, A.; Sharma, A. Enhanced Self-Organized Dewetting of Ultrathin Polymer Films Under Water-Organic Solutions: Fabrication of Sub-micrometer Spherical Lens Arrays. *Adv. Mater.* **2010**, *22*, 5306−5309.


DOI: 10.1021/la5045738
*Langmuir* 2015, 31, 3203−3214

(57) Verma, A.; Sharma, A. Submicrometer Pattern Fabrication by Intensification of Instability in Ultrathin Polymer Films under a Water-Solvent Mix. *Macromolecules* **2011**, *44*, 4928−4935.
(58) Ravi, B.; Mukherjee, R.; Bandyopadhyay, D. Solvent Vapour Mediated Spontaneous Healing of Self-organized Defects of Liquid Crystal Films. *Soft Matter* **2015**, *11*, 139−146.
(59) Ghatak, A.; Khanna, R.; Sharma, A. Dynamics and Morphology of Holes in Dewetting of Thin Films. *J. Colloid Interface Sci.* **1999**, *212*, 483−494.
(60) Huang, H.; Pan, L.; Lim, C. K.; Gong, H.; Guo, J.; Tse, M. S.; Tan, O. K. Hydrothermal Growth of $TiO_2$ Nanorod Arrays and in Situ Conversion to Nanotube Arrays for Highly Efficient Quantum Dot-Sensitized Solar Cells. *Small* **2013**, *9*, 3153−3160.
(61) Pfadler, T.; Coric, M.; Palumbiny, M.; Jakowetz, A. C.; Strunk, K.-P.; Dorman, J. A.; Ehrenreich, P.; Wang, C.; Hexemer, A.; Png, R.-Q.; Ho, P. K. H.; Muller-Buschbaum, P.; Weickert, J.; Schmidt-Mende, L. Influence of Interfacial Area on Exciton Separation and Polaron Recombination in Nanostructured Bilayer All-Polymer Solar Cells. *ACS Nano* **2014**, *12*, 12397−12409.



DOI: 10.1021/la5045738
*Langmuir* 2015, 31, 3203−3214